DOI:
10.1109/ICRA.2016.7487702

Document Version
Peer reviewed version

A Geometry Deformation Model for Compound Continuum Manipulators with External Loading*

S.M.Hadi Sadati[1], Ali Shiva[1], Ahmad Ataka[1], S. Elnaz Naghibi[2], Ian. D. Walker[3], Kaspar Althoefer[1], and Thrishantha Nanayakkara[1]

***Abstract*—Complexity of soft continuum manipulators with hybrid and tuneable structures poses a challenging task to achieve an inverse kinematics model which is both precise and computationally efficient for control and optimization purposes. In this paper, a new method based on the principle of virtual work and a geometry deformation approach is presented for the inverse kinematics model of the STIFF-FLOP arm which is a pneumatically actuated continuum manipulator. We propose a simplified and computationally efficient yet accurate analytical solution to analyse the static behaviour of a compound soft manipulator in the presence of external and body forces which is verified against experimental data, showing promising agreement. In the process, we present a new modelling approach for braided soft extensor actuators. For the first time, our model predicts a simple analytical solution for the cross section deformation which is essential to control soft manipulators with regional tunable stiffness structure.**

I. Introduction

Interest in the continuum robot manipulators has increased rapidly in the recent years. Continuum robots feature a backbone structure inspired by biological counterparts like the octopus arm, chameleon tongue, and elephant's trunk, with the ability to bend at any point along the backbone [1]. In the last decade, the continuum robot design has been implemented in several works such as OctArm [2], Meshworm [3], Tendril [4], GoQBot [5] and snake-arms [6]. The kinematics and dynamics modelling of continuum robot also gained similar popularity in the last decade. In [7], Webster and Jones reviewed several approaches for kinematic modelling of continuum robots based on constant curvature assumption using two consecutive separate sub mappings: one that is robot-specific, and another that is general and applies to all continuum robots. However, the robot-independent mapping could suffer from singularity, as addressed in studies such as [8], where a new shape function approach introduced by Godage overcomes this limitation. It is noted however, that the presence of external forces invalidates constant curvature assumptions in most cases, yet it is being used widely as a simplifying assumption. Dynamic models proposed recently can be divided into three categories: 1) Lumped model elements using Lagrangian representation, which consider a combination of rigid-link slices connected with spring and dampers such as in [9], where the total kinetic energy is derived by utilizing the limit operation as the degrees of freedom go to infinity for a planar 3-link continuum manipulator. 2) Cosserat rod model, as employed in [10] which results in a boundary condition problem in which Tunay solves the weak-form integral equations in a finite element discretization problem. 3) Approximate solutions based on identification of the system with a simple polynomial [11], or more recent solutions such as shape function based series [8] which results in a setup-specific model. The approximate solutions, suitable for control applications, are more accurate and improve the performance but do not incorporate the structural characteristics, while the lumped model element and Cosserat rod method, suitable for design and optimization, suffer from cumbersome calculations. Most of these methods suffer from numerical inaccuracy and singularities in deriving the inverse kinematics which is an essential part of a control system. Furthermore, force control is vital in medical, aerospace and human-robot interaction applications. To this end, stiffness-tuneable structures by granular jamming [12] and low-melting-point-alloys [13], morphing structures [14] and stiffness controllable interfaces by layer [15] and scale jamming [16] are recently investigated. This has resulted in compound inhomogeneous systems with modelling and control problems yet to be investigated.

To fill the gap between approximate and finite solutions, and constitute a base to model compound and tuneable stiffness structure manipulators, we propose a new approximate analytical method for the inverse kinematics based on the principle of virtual energy and Rivlin solution [17] for "the problem of flexure". In [17], Rivlin presents a geometrical approach to calculate the strain energy function of a cube made of an incompressible highly elastic material under pure elastic bending with certain geometrical assumptions about the relation of its deformed state to its initial state. Despite the semi-analytical method by Godage [8] which the shape function series solution for the forward kinematics and dynamics is based on the geometry of the manipulator, our model also accounts for incompressibility criteria and structural characteristics and results in a simple yet analytical solution for the inverse kinematics, making our model suitable for both design and control purposes. It should be noticed that although we used constant curvature assumptions in this paper, this is not a mandatory requirement and our

*Resrach supported by the Seventh Framework Program of the European Commission in the framework of EU project STIFF-FLOP, grant agreement 287728.

[1] S.M.Hadi Sadati, Ali Shiva, Ahmad Ataka, Kaspar Althoefer and Thrishantha Nanayakkara are with the Center for Robotics Research (CoRe), Department of Informatics, King's College London, London, WC2R 2LS, UK (email: seyedmohammadhadi.sadati@kcl.ac.uk, ali.shiva@kcl.ac.uk, kaspar.althoefer@kcl.ac.uk, thrish.antha@kcl.ac.uk.)

[2] S. E. Naghibi is with the Queen Mary, University of London, Department of Material and Mechanical Engineering, London, UK (email: naghibi@qmul.ac.uk).

[3] Ian D. Walker is with the Department of Electrical and Computer Engineering, Clemson University, Clemson, SC 29634. (e-mail: ngiri@clemson.edu; iwalker@clemson.edu).

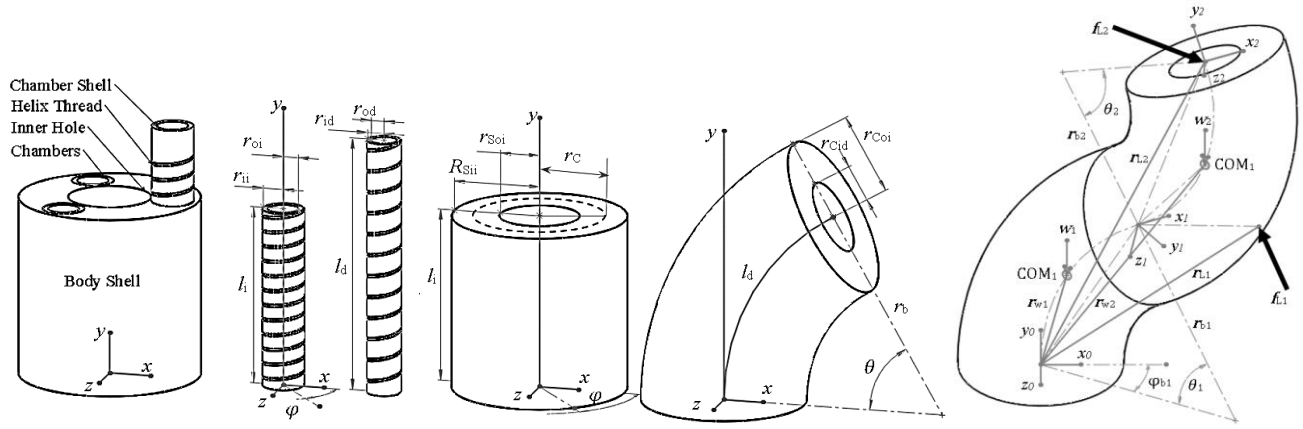

Figure 1. I & II) One STIFF-FLOP Module geometrical parameters before and after deformation. III) Reference frame and curvature parameters for a continuum manipulator consist of two STIFF-FLOP modules.

method can be derived assuming any shape function describing the deformation of the manipulator main axis. We study the modelling of the STIFF-FLOP soft modular manipulator for minimally invasive surgery [18]. This manipulator uses a braided pneumatic artificial muscle (PMA) similar to soft extensor actuators in OctArm [19] in the form of three parallel chambers and has an ability to undergo elongation and omnidirectional bending. Giri [20] used lumped model elements method and Trivedi [21] employed a more accurate but cumbersome Cosserat rod theory to model similar manipulators. The characteristic parameters of the chambers are not considered by Giri, while in [22] Trivedi uses a simple analytical map between the input pressure and elongation ratio for the chamber. There, it is assumed that all the chamber body elements are constrained to axial and circumferential deformation of the thread around the chamber, while their radial deformation is determined from incompressibility criteria. The model is simple and efficient; however, it does not consider the chamber bending and slip between the body and threads [21]. Our new modelling approach presented here addresses these limitations. In the sections II we discuss our modelling approach consisting of a geometrical map and a body-specific map. The body-specific map derivation is discussed based on our new geometry deformation approach for the bending soft body and actuator chamber in section III, followed by numerical simulation results in section IV and experiments on a manipulator consisting of two STIFF-FLOP modules in section V. Modeling and experimental reults comparison is discussed in section VI followed by a conclusion on our research and our future plan in section VII.

II. MODELLING

The STIFF-FLOP manipulator is assembled of separate modules, each consisting of three parallel penumatic soft extensor chambers covered in a soft silicon body (Fig. 1.I). Assuming constant curvature for deformations [7], the map between the system inputs (actuator chambers' pressures, $\boldsymbol{p}$) and outputs (manipulator tip position and orientation, $\boldsymbol{\rho}_{\mathbf{tip}}$) is given by $\boldsymbol{\rho}_{\text{tip}} = \boldsymbol{f}(\boldsymbol{p}) = \boldsymbol{f}_{\text{G}}(\boldsymbol{f}_{\text{S}}(\boldsymbol{p}))$, where $\boldsymbol{f}_{\text{G}}(\boldsymbol{\xi}_n)$ is a geometric map between curvature parameters ($\boldsymbol{\xi} = [\kappa, \phi, l]$, $\kappa = 1/r_{\text{b}}$) and manipulator tip position ($\boldsymbol{\rho}_{\text{tip}} = [x_{\text{t}}, y_{\text{t}}, z_{\text{t}}]$), κ is the curvature, ϕ is the bending direction angle, l is the curve length (Fig. 1.III) and $\boldsymbol{\xi} = \boldsymbol{f}_{\text{S}}(\boldsymbol{p})$ is a structural specific map between the $\boldsymbol{p}$ and $\boldsymbol{\xi}$. Having each module relative tip position expressed in its local frame, we can find $\boldsymbol{f}$ for each module separately. For the control purpose we need to find the inverse map between the system input and output vectors.

A. Geometrical Map ($\boldsymbol{f}_{\text{G}}$)

$\boldsymbol{f}_{\text{G}}$ for each module can be found from constant curvature assumptions [7] using a set of transformations given by $\mathbf{R}_y(\phi)$-$\mathbf{R}_z(\theta)$-$\boldsymbol{\rho}_{\text{T}}$-$\mathbf{R}_y(-\phi)$, where

$$\mathbf{R}_y(\phi_n) = \begin{bmatrix} \text{C}_{\phi_n} & 0 & \text{S}_{\phi_n} \\ 0 & 1 & 0 \\ -\text{S}_{\phi_n} & 0 & \text{C}_{\phi_n} \end{bmatrix},\ \mathbf{R}_z(\theta_n) = \begin{bmatrix} \text{C}_{\theta_n} & -\text{S}_{\theta_n} & 0 \\ \text{S}_{\theta_n} & \text{C}_{\theta_n} & 0 \\ 0 & 0 & 1 \end{bmatrix},$$
$$\boldsymbol{\rho}_{\text{T}n} = [(1-\text{C}_{\kappa_n l_n})/\kappa_n \quad \text{S}_{\kappa_n l_n}/\kappa_n \quad 0]^{\text{T}}, \quad (1)$$

$\theta = \kappa.l$ is the module arc angle, $\mathbf{R}_a(b)$ is the rotation matrix for a rotation of b around axis a and $\boldsymbol{\rho}_{\text{T}}$ is the translation vector in local xyz coordinates. We use C_x for $\cos(x)$ and S_x for $\sin(x)$. The transformation matrix for each module ($\boldsymbol{T}_n$) is

$$\boldsymbol{T}_n(\kappa_n, \phi_n, l_n) = \begin{bmatrix} \mathbf{R}_y(\phi_n) & 0 \\ 0 & 1 \end{bmatrix} . \begin{bmatrix} \mathbf{R}_z(\theta_n) & \boldsymbol{\rho}_{\text{T}n} \\ 0 & 1 \end{bmatrix} \begin{bmatrix} \mathbf{R}_y(-\phi_n) & 0 \\ 0 & 1 \end{bmatrix}, (2)$$

where subscrit n is the modue number starting from the base module. The inverse map ($\boldsymbol{f}_{\text{G}}^{-1}$) between $\boldsymbol{\xi}$ and $\boldsymbol{\rho}_{\mathbf{tip}}$ is

$$\boldsymbol{f}_{\text{G}}^{-1} = \begin{cases} \phi_n = \text{atan}(z_{\text{t}n}/x_{\text{t}n}) \\ \theta_n = \kappa_n l_n = 2\,\text{atan}(\sqrt{x_{\text{t}n}^2 + z_{\text{t}n}^2}/y_{\text{t}n}) \\ \kappa_n = \text{S}_{\theta_n}/y_{\text{t}n} \end{cases}. (3)$$

The chambers' arc length (l_{C}) become

$$\begin{cases} l_{\text{C}1} = l_n(1 - \kappa_n r_{\text{C}n}\text{C}_{(-\phi_n)}) \\ l_{\text{C}2} = l_n(1 - \kappa_n r_{\text{C}n}\text{C}_{(-\phi_n+2\pi/3)}), \\ l_{\text{C}3} = l_n(1 - \kappa_n r_{\text{C}n}\text{C}_{(-\phi_n-2\pi/3)}) \end{cases} \quad (4)$$

where r_{C} is the radius of the circle passing through chambers axes where $l_{\text{C}1}$ is located on the module local frame x axis and $l_{\text{C}2}$ and $l_{\text{C}3}$ are located with $2\pi/3$ ofsset in c.c.w. direction.

B. Structural Specific Map ($\boldsymbol{f}_{\text{S}}$)

We use the principle of virtual work which provides an easy energy-based model to find $\boldsymbol{f}_{\text{S}}$. It states that the summation of all works and stored energies of all the elements in a system remains zero during any infinitesimal virtual displacement. To derive this, we calculate the work done by the external loads

(∂w_L), potential energy change due to work done by body forces such as gravity (∂w_w), change in energy stored in the module body shell (∂w_S), change in energy stored in all chambers (∂w_C) and work done by the chambers' air presure (∂w_G). Hence, the principle of virtual work for the system is,

$$\partial w_L + \partial w_w + \partial w_S + \partial w_C + \partial w_G = 0 \qquad (5)$$

which can be derived for each module seperatly, acounting the next modules attached to the tip as external loads. For the external load (∂w_L) and body forces (∂w_w), we sum the inner product of each external force vector (f_{Li}) with its exerting point absolute position vector ($\boldsymbol{\rho}_{Ln}$) and differentiate it w.r.t. the module curvature parameters ($\boldsymbol{\xi}_n$) to obtain ∂w_L as:

$$\partial w_L = \sum_j \boldsymbol{f}_{Lj}.\delta\boldsymbol{\rho}_{Lj}/\partial\xi_n. \qquad (6)$$

where subscript j denotes the external force number. The same can be done for body forces ($\boldsymbol{w}_n$),

$$\partial w_w = \sum_{k=n}^{n_e} \boldsymbol{w}_k.\delta\boldsymbol{\rho}_{wk}/\partial\xi_n, \qquad (7)$$

where $\boldsymbol{\rho}_{wj}$ is the centre of mass (COM) absolute position vector, subscript n denotes the module number that we solve Eq. 5 for, subscript k denotes the module number starting from n (the current module) to n_e (the last module attached at the end of the current module). The absolute position vectors (w.r.t. and expressed in the reference frame) are derived by transformation matrices (Eq. 2) post multiplication rule,

$$\boldsymbol{\rho}_{wk} = (\prod_{m=1}^{k-1}\boldsymbol{T}_m)\boldsymbol{\rho}_{wrk},\ \boldsymbol{\rho}_{Lj} = (\prod_{m=1}^{k-1}\boldsymbol{T}_m)\boldsymbol{\rho}_{Lrj}, \qquad (8)$$

where $\boldsymbol{\rho}_{Lrj}$ and $\boldsymbol{\rho}_{wrk}$ are the local position vectors (w.r.t. and expressed in local frame) and k is the module number to which the j^{th} external load is exerted or the k^{th} COM is attached. We assume the COM is located at the middle of each module axial curve ($\boldsymbol{\rho}_{wrn} = \boldsymbol{T}_i(\kappa_n,\phi_n,l_n/2).[0, 0, 0, 1]^T$). We use a new method based on early works by Rivlin in [17] to derive ∂w_S and ∂w_C which we name "Geometry Deformation Method".

III. Geometry Deformation Model

If we derive the map between the initial and deformed state of an incompressible highly elastic body in the same coordinate system, we can derive the strain matrix and use its invariants to find the deformation energy. We use a similar approach as Rivlin's solution for "The problem of flexure" [17] to calculate the energy stored in body shell (∂w_S) and actuator chambers (∂w_C). We consider the same assumptions by Rivlin for our body shell in elongation and bending and solve it for a hollow cylinder, which gives us a simple analytical solution. We use the same method to derive the stored energy in an actuator chamber for pure elongation to get a simplified analytical solution. Then the virtual energy equals to the stored energy differentiation w.r.t. module curvature parameters.

A. Elongation-Bending of Body Shell (Simplified Case)

We chose to present the initial and deformed states in Cartesian coordinates. However, we can break the transformation to a set of transformations between different coordinate systems to simplify the procedure. Here, subscript i stands for initial state, d stands for transformations to deformed states. An added t in the subscript stands for intermediate transformations in initial or final states. The initial state, $\boldsymbol{\rho}_i = (x, y, z)$, is presented in Cartesian coordinates and the deformed state, $\boldsymbol{\rho}_{td} = (r^*, \theta, z)$, is presented in cylindrical coordinates. We can assume based on observation that r^* is only a function of x, θ is only a function of y and there is no deformation in the z direction. Finally, a transformation is used to present the deformed state, $\boldsymbol{\rho}_d = (x_d, y_d, z_d)$, in Cartesian coordinates. The full body specific map becomes, $\boldsymbol{f}_S = \boldsymbol{\rho}_d(\boldsymbol{\rho}_{td}(\boldsymbol{\rho}_i))$ expanded as,

$$\rho_i = \begin{pmatrix} x \\ y \\ z \end{pmatrix},\ \rho_{td} = \begin{pmatrix} r^*(x) \\ \theta(y) \\ z \end{pmatrix},\ \rho_d = \begin{pmatrix} x_d = r^*(x)\,C_{\theta(y)} - r_b \\ y_d = r^*(x)\,S_{\theta(y)} \\ z_d = z \end{pmatrix}, \qquad (9)$$

where $r^*(x)$ and $\theta(y)$ are so far undetermined, and in order to find a general function form we use the incompressibility criteria as in [17]. The incompressibility criteria can be satisfied if the determinant of the Jacobian of the deformed state map ($\boldsymbol{\rho}_d$) w.r.t. initial states ($\boldsymbol{\rho}_i$) becomes unity as follows,

$$\det\left(\frac{\partial\rho_d}{\partial\rho_i}\right) = \det\left(\begin{bmatrix} r^*_{,x}C_\theta & -r^*\theta_{,y}S_\theta & 0 \\ r^*_{,x}S_\theta & r^*\theta_{,y}C_\theta & 0 \\ 0 & 0 & 1 \end{bmatrix}\right) = r^* r^*_{,x}\theta_{,y} = 1. \qquad (10)$$

where $a_{,b}$ stands for $\partial a/\partial b$. We use separation of variables to get the following two differential equations,

$$\begin{cases} \frac{\partial}{\partial x}\left(\frac{1}{r^* r^*_{,x}}\right) = 0 \rightarrow r^*(x) = (2A_1 x + A_2)^{1/2} \\ \frac{\partial}{\partial y}(\theta_{,y}) = 0 \rightarrow \theta(y) = A_3 y + A_4 \end{cases}, \qquad (11)$$

$$\rightarrow r^* r^*_{,x}\theta_{,y} = A_1 A_3 = 1 \rightarrow A_1 = 1/A_3, \qquad (12)$$

where A_i can be found from boundary conditions. The bending angle (θ) at the module bottom ($y = 0$) is zero, then $A_4 = 0$, and for θ at the tip ($y = l$) we have $r_b\theta(l) = l_d$, then $A_3 = \lambda_1/r_b$ and $A_1 = r_b/\lambda_1$, where $\lambda_1 = l_d/l_i$ is the axial length deformation rate and l_i and l_d are the module axis initial and deformed length. We assume r_b is the radius of curvature for the cylinder central axis at ($x = 0$) to solve for A_2 as follows

$$r^*(0) = A_2^{1/2} = r_b \rightarrow A_2 = r_b^2. \qquad (13)$$

Finally, we obtain to the following relation for r^*,

$$r^*(x) = (2xr_b/\lambda_1 + r_b^2)^{1/2}, \qquad (14)$$

The deformation map ($\boldsymbol{\rho}_i$-$\boldsymbol{\rho}_d = (u, v, w)$), which is needed to derive the strain matrix and its invariants, is

$$u = x_d - x,\ v = y_d - y,\ w = z_d - z = 0,$$
$$u = (2xr_b/\lambda_1) + r_b^2)^{1/2}C_{(\lambda_1 z/r_b)} - r_b - x,$$
$$v = (2xr_b/\lambda_1 + r_b^2)^{1/2}S_{(\lambda_1 z/r_b)} - y. \qquad (15)$$

B. Soft Actuator Model in Elongation

Energy stored in a threaded pneumatic chamber such as a McKibben actuator in elongation has been investigated in literature assuming that the chamber shell elements follow the thread shape[21][22]. It is assumed that the constant length of thread constrains the axial (λ_1) and circumferential deformation rate ($\lambda_3 = r_{cd}d\phi_d/(r_{ci}d\phi_i)$) of the cylinder as, $\lambda_3^2 S_{\gamma_i}^2 + \lambda_1^2 C_{\gamma_i}^2 = 1$, where r_c is the thread helix inner radius. This provides a simple analytical solution for the energy stored due to elongation in the shell. However, the slip between the body shell and the threads causes inaccuracy of the model prediction [21]. We use the same procedure as in the previous section to solve this problem in a new way. We assume the

shell outer diameter is constrained to the thread helix radius and the shell elements does not twist ($\phi_d = \phi_i = \phi$) but can slip axially against the wall. The no-twist assumption results in $\lambda_3 = \lambda_2 = r_{cd}/r_{ci}$, handing in a new more accurate analytical solution. To this end, we assume a map from Cartesian ($\boldsymbol{\rho}_i = [x, y, z]$) to cylindrical coordinates ($\boldsymbol{\rho}_{ti} = [r, y, \phi]$) in initial state, followed by a map to the deformed state in cylindrical coordinates ($\boldsymbol{\rho}_{td} = [r_d, y_d, \phi_d]$), where we assume r_d is only a function of r and undetermined so far. Finally, we have a map to express the deformed state in Cartesian coordinates ($\boldsymbol{\rho}_d = [x_d, y_d, z_d]$). The expanded full map function becomes

$$\rho_i = \begin{pmatrix} x \\ y \\ z \end{pmatrix}, \rho_{ti} = \begin{pmatrix} r \\ y \\ \phi \end{pmatrix}, \rho_{td} = \begin{pmatrix} r_d(r) \\ y_{td} = \lambda_1 y \\ \phi_d = \phi \end{pmatrix}, \rho_d = \begin{pmatrix} x_d = r_d C_\phi \\ y_d = y_{td} \\ z_d = r_d S_\phi \end{pmatrix}, \quad (16)$$

Using incompressibility criteria to find a general function form for r_d, we have

$$\det\left(\frac{\partial \boldsymbol{\rho}_d}{\partial \boldsymbol{\rho}_i}\right) = \det\left(\frac{\partial \boldsymbol{\rho}_d}{\partial \boldsymbol{\rho}_{td}}\right).\det\left(\frac{\partial \boldsymbol{\rho}_{td}}{\partial \boldsymbol{\rho}_{ti}}\right).\det\left(\frac{\partial \boldsymbol{\rho}_{ti}}{\partial \boldsymbol{\rho}_i}\right) = 1, \quad (17)$$

For transformations between cylindrical and Cartesian coordinates with no deformation we have, $\det(\partial \boldsymbol{\rho}_{ti}/\partial \boldsymbol{\rho}_i) = 1/r$ and $\det(\partial \boldsymbol{\rho}_d/\partial \boldsymbol{\rho}_{td}) = r_d$. Substituting these in 20 we get

$$\det\left(\frac{\partial \boldsymbol{\rho}_{td}}{\partial \boldsymbol{\rho}_{ti}}\right) = \begin{bmatrix} r_{d,r} & 0 & 0 \\ 0 & \lambda_1 & 0 \\ 0 & 0 & 1 \end{bmatrix} = r_{d,r}\lambda_1 = \frac{r}{r_d}, \quad (18)$$

Solving the resulting differential equation, we have,

$$\int r_d \mathrm{d}r_d = \int r/\lambda_1 \, \mathrm{d}r \rightarrow r_d = \sqrt{r^2/\lambda_1 + A_1}, \quad (19)$$

where A_1 can be found based on boundary conditions. The chamber outer radius in deformed state ($r_d(r_{i2})$) should be equal to thread helix radius ($r_c = r_d(r_{i2}) = \lambda_2 r_{i2}$). Then we have,

$$r_c = \sqrt{r_{i2}^2/\lambda_1 + A_1} \rightarrow A_1 = r_c^2 - r_{i2}^2/\lambda_1, \quad (20)$$

where r_{i2} is the chamber initial outer radius. The deformation map $\boldsymbol{\rho}_d$-$\boldsymbol{\rho}_i = (u, v, w)$ is,

$$u = \sqrt{r_{i2}^2/\lambda_1 + r_c^2 - r_{i2}^2/\lambda_1}\, C_\phi - x, \; v = \lambda_1 y - y,$$
$$w = \sqrt{r_{i2}^2/\lambda_1 + r_c^2 - r_{i2}^2/\lambda_1}\, S_\phi - z. \quad (21)$$

C. Strain Matrix Invariants and Deformation Energy

We derive the deformation energy (w_S and w_C) based on Neo-Hookean model [21][23], $w_{S \text{ or } C} = E I_{1S \text{ or } C}/6$, where I_1 is the deformation matrix first invariants and E is the material module of elasticity. The elements on the main axis of the deformation matrix (e_{xx}, e_{yy} and e_{zz}) are needed to find I_1 which we derive based on the deformation map as in [24],

$$e_{xx} = u_{,x} + \left(u_{,x}^2 + v_{,x}^2 + w_{,x}^2\right)/2,$$
$$e_{yy} = v_{,y} + \left(u_{,y}^2 + v_{,y}^2 + w_{,y}^2\right)/2,$$
$$e_{zz} = w_{,z} + \left(u_{,z}^2 + v_{,z}^2 + w_{,z}^2\right)/2, \quad (22)$$
$$I_1 = 3 + 2\left(e_{xx} + e_{yy} + e_{zz}\right). \quad (23)$$

The deformation matrix first invariants for each point of the body shell (dI_{1S}) is found by substituting Eq. 15 in 22 and 23

$$dI_{1S} = \lambda_1^2 + r_b/(\lambda_1(2x + r_b\lambda_1)) + (2\lambda_1 x)/r_b + 1, \quad (24)$$

where we need to integrate over the initial body volume domain (v_i) and use the Neo-Hookean model to find the strain energy stored in the deformed body (w_S),

$$w_S = \frac{E}{6}\int_{v_i} dI_{1s}\, dv = \frac{2 l_i E}{6}\int_{-r_i}^{r_i}\int_0^{\sqrt{r^2-x^2}} dI_{1s}\, dy dx, \quad (25)$$

We use binomial expansion for square root up to two terms to get a simple analytical solution for the integral ($(r^2\text{-}x^2)^{1/2} \approx r(1\text{-}0.5r^2/x^2)$. Our simulations show more terms do not increase the integration accuracy significantly. Solving Eq. 25 we get,

$$w_S(r) = \frac{E}{6}\left(\frac{12 r_b^2 r + r^3(80(1+\lambda_1) - 3\lambda_1 A_2) + 3 r_b^3 \lambda_1 A_1}{24 r} + \frac{r_b r (A_2 - A_1)}{\lambda_1}\right),$$
$$A_1 = \log(r_b\lambda_1/2 - r), \; A_2 = \log(r_b\lambda_1/2 + r). \quad (26)$$

Substituting Eq. 26 in the Neo-Hookean model, for a hollow cylinder with r_{si1} as the body shell initial inner radius and r_{si2} as its initial outer radius, ∂w_S is

$$\partial w_S = \partial\left(w_S(r_{Si2}) - w_S(r_{Si1})\right)/\partial \boldsymbol{\xi}_n. \quad (27)$$

For the chamber body deformation energy (w_C) by substituting Eq. 21 in 22 and 23 and integrating over the initial volume domain in cylindrical coordinates, we have

$$w_C = \frac{E}{6}\int_{v_i} dI_{1C}\, dv = \frac{2 l_i E}{6}\int_{r_{i1}}^{r_{i2}}\int_0^{\pi} dI_{1C}\, r d\phi dr, \quad (28)$$

where r_{i1} is the chamber inner radius and r_{i2} is its initial outer radius. We can assume $\gamma_i \approx \pi/2$ or $\lambda_2 \approx 1$, then for dI_{1C} we get

$$dI_{1C} = \frac{\lambda_1^2 x^2 + \lambda_1^2 z^2 + r_{i2}^2}{x^2 + z^2} + \frac{r_{i2}^4 - 2 r_{i2}^2 x^2 - 2 r_{i2}^2 z^2 + 2x^4 + 4x^2 z^2 + 2z^4}{\lambda_1 (x^2 + z^2)(-r_{i2}^2 + x^2 + z^2)} -$$
$$\frac{r_{i2}^2 (x^2 + z^2)}{(-r_{i2}^2 + x^2 + z^2)(\lambda_1 r_{i2}^2 - r_{i2}^2 + x^2 + z^2)}. \quad (29)$$

Substituting Eq. 29 in 27

$$w_C(r) = \frac{2\pi l_0 E}{6\lambda_1}\left(r(2 + \lambda_1^3) - r_{i2}\sqrt{1 - \lambda_1}\tanh^{-1}\left(\frac{r}{r_{i2}\sqrt{1-\lambda_1}}\right) - \frac{r_{i2}^2(\lambda_1 - 1)}{r}\right), \quad (30)$$

Using Eq. 30, for ∂w_C we have,

$$\partial w_C = \partial\left(w_C(r_{i2}) - w_C(r_{i1})\right)/\partial \boldsymbol{\xi}_n. \quad (31)$$

D. Gas Virtual Work Energy

The virtual work of gas inside the chambers is,

$$\partial w_G = \partial(\boldsymbol{p}\boldsymbol{v}_C)/\partial \boldsymbol{\xi}_n, \quad (32)$$

where $\boldsymbol{v}_C$ is the three deformed chambers internal volume vector. Assuming uniform cross section along the main axis and the deformed chamber cross section area is

$$v_C = \pi l_0 \lambda_1 \sqrt{\left((r_{ii}^2 - r_{oi}^2)/\lambda_1 + r_{oi}^2\left(\lambda_1^2 C_{\gamma_o}^2 - 1\right)^2/S_{\gamma_i}^4\right)}, \quad (33)$$

and For the simplified case ($\lambda_2 \approx 1$) we have,

$$v_C = \pi l_0 \lambda_1 \sqrt{(r_{ii}^2 - r_{oi}^2)/\lambda_1 + r_{oi}^2}. \quad (34)$$

A model for a braided soft extensor actuator in elongation can be derived from Eq. 31-34 as, $p = (\partial w_C/\partial \lambda_1)/(\partial v_C/\partial \lambda_1)$.

IV. Numerical Simulation

Despite the mathematical background, the final derived analytical model is simpler and easier to implement in comparison to other modelling approaches in literature such as [8],[9],[10]. Substituting Eq.s 6-8, 26, 27, 30-32 and 34 in Eq. 5 gives a simplified analytical model assuming $\lambda_2 \approx 1$. An

exact model is derived by substituting Eq. 30 with integration of Eq. 28. After deducing the deformation energy of the chamber holes, we set the coefficient of each element of ∂ to be zero in Eq. 5. This gives a system of three equations of the form $\boldsymbol{A}.\boldsymbol{p} = \boldsymbol{b}(\boldsymbol{\xi})$, where from Eq. 32, $\boldsymbol{A} = \partial \boldsymbol{v}_C/\partial \boldsymbol{\xi}$ and $\boldsymbol{b}(\boldsymbol{\xi})$ is the vector of the remaining terms. This solves $\boldsymbol{p}$ as a nonlinear function of $\boldsymbol{\xi}$ for each module ($\boldsymbol{p} = \mathbf{A}^{-1}.\mathbf{B}(\boldsymbol{\xi}) = \boldsymbol{f}_S^{-1}(\boldsymbol{\xi})$) which is the inverse of the structural specific map ($\boldsymbol{f}_S^{-1}$). We simulate the static behaviour of a soft manipulator consist of two STIFF-FLOP modules in 15 different arbitrary orientations as in Fig. 3. Curvature parameters for each module is found by substituting the tip positions from the experiments in Eq. 3 and then Eq. 4. The body specific map as in section III.E is used to model the required pressure inputs. For verification purposes, one chamber in module 2 is set to zero intentionally. The force sensor weight is modelled as an external force while the inverse and Jacobian matrices are calculated numerically. We use the data from 8 experiment points to identify two sets of parameters for the modules using our main model as in Table 1 where module 1 is attached to the base. The identified parameters are consistent with our actual measurements. The elasticity of the soft media is less than the manufacturing data sheet values due to air bubbles remained from the moulding process. The simulation results for both models in comparison to experimental measurements are presented in Fig 4.

V. Experiments

As explained in [18], the STIFF-FLOP manipulator is a soft continuum manipulator designed for minimally invasive surgery (MIS), consisting of modules as building blocks. Each module is a silicon based cylinder (Ecoflex 50, tensile strength 2.17 [MPa]). At the center of the cylinder there is hollow passage in order to accommodate necessary cables for sensors and air supply pipes of the following mounting modules. The manipulator in this study is composed of two serially linked modules. In the periphery of each module, three dual fluidic pressure chambers are implemented for pneumatic actuation. These chambers are aligned with the module's main longitudinal axis and oriented at 120 [deg] from each other. Each chamber is braided using a normal thread wound around its body which would allow axial elongation whilst constraining radial inflation. The module bend when the air pressure in one dual chamber is increased more than the other two dual chambers. Simultaneous pressurization of the all dual chambers would cause an overall elongation of one module. To provide the desired pressure value, the STIFF-FLOP manipulator is connected to pressure regulators, a compressor, and a computer as depicted in Fig. 2. A data acquisition board (RoNeX) provides the desired PWM voltage for the pressure valves to regulate the pressure via electronic proportional micro pressure regulators

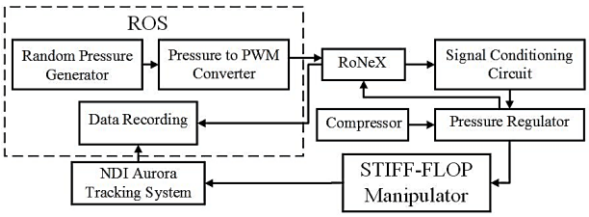

Figure 2. Experiment setup and control system diagram.

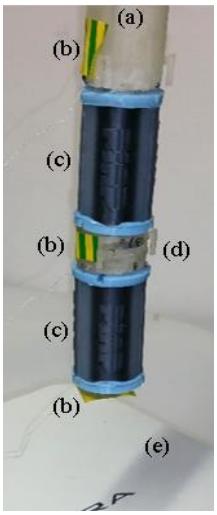

Table 1. Simulation parameters based on identification and measurements on experiment setup.

Par.	Mod. 1	Mod. 2
r_{ii} [mm]	6.0	3.5
r_{oi} [mm]	9.2	3.1
γ_0 [deg]	89.9	80.7
r_C [mm]	12.2	13.1
r_{Soi} [mm]	2.5	7.3
r_{Sii} [mm]	14.1	14.8
l_i [mm]	20.0	28.2
l_{fs}^* [mm]	0.0	30.0
E [KPa]	17.324	17.317
w [N]	0.039×g	0.020×g
f_L [N]	0.014×g	0
g^* [m/s^2]	9.81	9.81
ϕ_b^* [deg]	-31.2	2.4

* l_{fs} is the force sensor axial length, g is the gravity acceleration coefficient, ϕ_b is the initial relative rotation of each module local frame around local y axis.

Figure 3. Experimental setup, (a) base, (b) Aurora sensor coil, (c) STIFF-FLOP modules, (d) force sensor, (e) Aurora Tracking System.

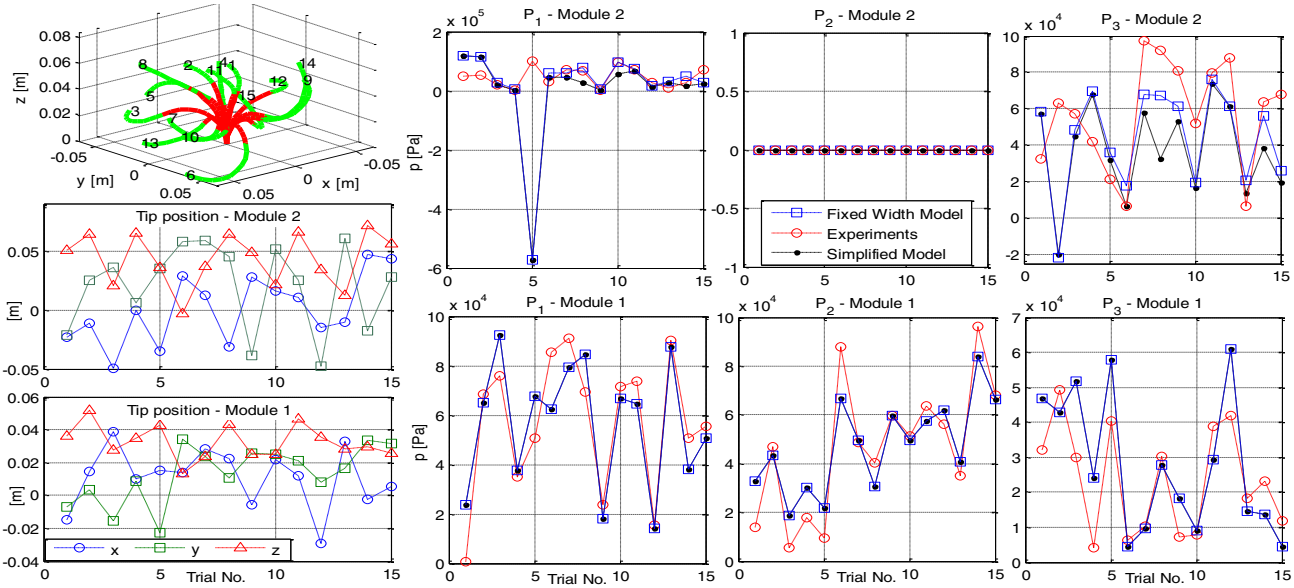

Figure 4. Simulation results of inverse full map to find input pressures to reach certain tip positions in comparison to actual pressures results from experiments for 15 arbitrary trials. 8 trials (no. 3, 4, 6, 8, 10, 11, 13 and 15) are used for training. Module 1 is the bottom module.

(Camozzi K8P) connected to the compressor (BAMBI MD Range Model 150/500). To validate our model, we give a series of random input pressures to the system, ranging from 0 to 0.1 [MPa], and record the position of three electromagnetic-based sensor coils located at the base, middle, and tip of the manipulator via the NDI Aurora tracking system.

VI. DISCUSSION

The comparison between the simulation and experimental results are presented in Fig. 4. Both models are almost identical for the first module while their difference is more obvious for the second module with smaller γ_0. The mean error of main method results for both modules are 9.4 and 29.7 [KPa] respectively while this error for the 8 trials used for parameter identification is 9 and 11.6 [KPa]. The models are reasonably accurate in predicting the first module behavior which constant curvature assumptions results in less errors. This is mainly because the modules are not symmetric and identical because our current fabrication process of the modules does not generate consistent module structural properties, hence they may not obey the constant curvature and fixed width assumptions. The offsets between the tracking sensors and the modules main axis (Fig. 3) cause reading error too. These errors accumulate for the second chamber, causing more modelling error. Besides, we assume uniform cross section along the module and neglect the interaction of the body shell and actuator surfaces. The agreement is better when all chambers are pressurized since the model assumes the gas inside the chambers has always an active effect on its internal volume. The chamber volume undergoes passive deformations which our model does not capture (trial no. 5 in module 2). We plan to address these issues by using a general shape function instead of constant curvature assumption and presenting a general solution which considers the actuator chamber bending and non-uniform deformation of the soft material cross sections.

VII. CONCLUSIONS

We introduced a new efficient analytical approach to model compound continuum manipulators with external and body forces based on principle of virtual work and experimental observation of the deformed system with constant curvature as a preliminary but not necessary assumption. A set of assumptions, based on observation of a deformed soft manipulator, gives us a framework to derive the analytical deformation map of the system incorporating its compound structural characteristics and capable of predicting the cross sectional deformation which we showed to be valid when the constant curvature assumption holds in comparison to experimental data. We present a new model for braided soft extensor actuators without restricting surface-braids relative slip. We believe, this method has promising capabilities for both optimization and control purposes to fill the gap between simple non-accurate models and time consuming more accurate methods. The results can be used to model and control stiffness-tuneable structure manipulators with regional stiffness control in their cross section.

REFERENCES

[1] B. Siciliano and O. Khatib, *Springer handbook of robotics*. Springer Science & Business Media, 2008.

[2] W. McMahan, V. Chitrakaran, M. Csencsits, and others, "Field trials and testing of the OctArm continuum manipulator," in *Robotics and Automation, 2006. ICRA 2006. Proceedings 2006 IEEE International Conference on*, 2006, pp. 2336–2341.

[3] S. Seok, C. D. Onal, K.-J. Cho, and others, "Meshworm: a peristaltic soft robot with antagonistic nickel titanium coil actuators," *Mechatronics, IEEE/ASME Trans.*, vol. 18, no. 5, pp. 1485–1497, 2013.

[4] J. S. Mehling, M. Diftler, M. Chu, and others, "A minimally invasive tendril robot for in-space inspection," in *Biomedical Robotics and Biomechatronics, 2006. BioRob 2006. The First IEEE/RAS-EMBS International Conference on*, 2006, pp. 690–695.

[5] H.-T. Lin, G. G. Leisk, and B. Trimmer, "GoQBot: a caterpillar-inspired soft-bodied rolling robot," *Bioinspir. Biomim.*, vol. 6, no. 2, p. 26007, 2011.

[6] R. Buckingham, "Snake arm robots," *Ind. Robot An Int. J.*, vol. 29, no. 3, pp. 242–245, 2002.

[7] R. J. Webster and B. a. Jones, "Design and Kinematic Modeling of Constant Curvature Continuum Robots: A Review," *Int. J. Rob. Res.*, vol. 29, no. 13, pp. 1661–1683, Jun. 2010.

[8] I. S. Godage, D. T. Branson, E. Guglielmino, and others, "Shape function-based kinematics and dynamics for variable length continuum robotic arms," in *Robotics and Automation (ICRA), 2011 IEEE International Conference on*, 2011, pp. 452–457.

[9] E. Tatlicioglu, I. D. Walker, and D. M. Dawson, "Dynamic modelling for planar extensible continuum robot manipulators," in *Robotics and Automation, 2007 IEEE International Conference on*, 2007, pp. 1357–1362.

[10] I. Tunay, "Spatial continuum models of rods undergoing large deformation and inflation," *IEEE Trans. Robot.*, vol. 29, no. 2, pp. 297–307, 2013.

[11] G. Chen, M. T. Pham, and T. Redarce, "Sensor-based guidance control of a continuum robot for a semi-autonomous colonoscopy," *Rob. Auton. Syst.*, vol. 57, no. 6–7, pp. 712–722, 2009.

[12] E. Steltz, a. Mozeika, J. Rembisz, and others, "Jamming as an Enabling Technology for Soft Robotics," in *Spie*, 2010, vol. 7642, p. 764225.

[13] N. G. Cheng, A. Gopinath, L. Wang, and others, "Thermally Tunable, Self-Healing Composites for Soft Robotic Applications," *Macromol. Mater. Eng.*, pp. 1279–1284, 2014.

[14] I. K. Kuder, A. F. Arrieta, W. E. Raither, and P. Ermanni, "Variable stiffness material and structural concepts for morphing applications," *Prog. Aerosp. Sci.*, vol. 63, pp. 33–55, 2013.

[15] Y. J. Kim, S. Cheng, S. Kim, and K. Iagnemma, "Design of a tubular snake-like manipulator with stiffening capability by layer jamming," *IEEE Int. Conf. Intell. Robot. Syst.*, pp. 4251–4256, 2012.

[16] S. M. H. Sadati, Y. Noh, S. E. Naghibi, and others, "Stiffness Control of Soft Robotic Manipulator for Minimally Invasive Surgery (MIS) Using Scale Jamming," in *Intelligent Robotics and Applications*, Springer, 2015, pp. 141–151.

[17] R. S. Rivlin, "Large Elastic Deformations of Isotropic Materials. V. The Problem of Flexure," *Proc. R. Soc. A Math. Phys. Eng. Sci.*, vol. 195, no. 1043, pp. 463–473, 1949.

[18] M. Cianchetti, T. Ranzani, G. Gerboni, and others, "STIFF-FLOP surgical manipulator: mechanical design and experimental characterization of the single module," in *Intelligent Robots and Systems (IROS), 2013 IEEE/RSJ International Conference on*, 2013, pp. 3576–3581.

[19] D. Trivedi, A. Lotfi, and C. D. Rahn, "Geometrically exact models for soft robotic manipulators," *IEEE Int. Conf. Intell. Robot. Syst.*, vol. 24, no. 4, pp. 1497–1502, 2007.

[20] N. Giri and I. D. Walker, "Three module lumped element model of a continuum arm section," *IEEE Int. Conf. Intell. Robot. Syst.*, pp. 4060–4065, 2011.

[21] D. Trivedi, A. Lotfi, and C. D. Rahn, "Geometrically exact models for soft robotic manipulators," *Robot. IEEE Trans.*, vol. 24, no. 4, pp. 773–780, 2008.

[22] W. Liu and C. R. Rahn, "Fiber-Reinforced Membrane Models of McKibben Actuators," *J. Appl. Mech.*, vol. 70, no. 6, p. 853, 2003.

[23] A. N. Gent, *Engineering with rubber: how to design rubber components*, 3rd ed., vol. 59, no. 3. Munich: Carl Hanser Verlag GmbH Co KG, 2012.

[24] R. S. Rivlin, "Large Elastic Deformations of Isotropic Materials. IV. Further Developments of the General Theory," *Philos. Trans. R. Soc. A Math. Phys. Eng. Sci.*, vol. 241, no. 835, pp. 379–397, 1948.